Proceedings of the 2^{nd} International Conference on Porous Media and its Applications in Science and Engineering
ICPM2
June 17-21, 2007, Kauai, Hawaii, USA

Wicking of Perfectly Wetting Liquids into a Metallic Mesh

N. Fries, K. Odic and M. Dreyer
Center of Applied Space Technology and Microgravity (ZARM), University of Bremen. Am Fallturm, 28359 Bremen, Germany, E-mail of the corresponding author: dreyer@zarm.uni-bremen.de

Abstract

Imbibition of liquids into porous media has significant importance to many processes. For example one application is the propellant management device (PMD), or liquid acquisition device (LAD), located within spacecraft tanks [1, 7]. The PMDs are designed to ensure gas free delivery of propellant during all mission accelerations. This is done by using a porous medium, a metallic mesh, which prevents gas from entering due to its bubble point. In this study the wicking of different liquids into a Dutch-Twilled-Weave (DTW) 200×1400 screen is analyzed by combining experimental and numerical approaches. The imbibition experiments were performed under isothermal and terrestrial conditions. Video recordings have been analyzed in order to study the wicking behavior in terms of liquid rise over time. Out of this evaluation mesh pore structure parameters could be determined. The well-known Lucas-Washburn equation was used, while its limitations under the influence of gravity are pointed out.

INTRODUCTION

The main issue when dealing with the functionality of spacecraft propellant tanks is the lack of gravity to define "up" and "down". The propellant management devices (PMDs) are designed to ensure a constant connection between the propellant and the outlet (communication type) or a localization and confinement of the propellant at a designated location (control type) [14]. Fig. 1 shows that a total communication type PMD includes a network of galleries made of fine porous mesh screens (Fig. 2) running through it. They are passive surface tension devices, which provide gas free propellant during all mission accelerations. This requires that the screens are always saturated with propellant. If any drying has occurred, wicking can be regarded as a self healing process to replace liquid and restore operation. The research conducted aims to provide more insight into this phenomenon.

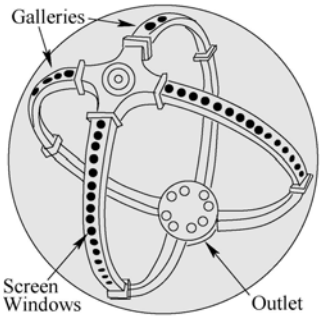

Figure 1: Propellant management device [5].

NOMENCLATURE

a	Constant Eq.(11)/ FLOW-3D coefficient
A_p	Pore area [m^2]
b	Constant Eq.(12)/ FLOW-3D coefficient
B_s	Screen thickness [m]
Bo	Bond number: Bo= $\rho g D_s^2/4\sigma$
C_w	Wicking friction parameter
D_{BP}	Bubble point diameter [m]
D_e	Effective diameter [m], $D_e = D_h^2/D_s$
D_h	Hydraulic diameter, $D_h = 4A_p/P_p$ [m]
D_s	Static Diameter [m]
g	Gravity [m/s^2]
h	Liquid front height [m]: $h = h_l + h_0 + h_w$
h_c	Characteristic height [m]
h_l	Depth of immersion [m]
h_0	Height of the mesh covered by wetting [m]
$h_{\max}$	Maximum liquid front height [m]
h_w	Height of the wicking front [m]
H_m	Height of the mesh [m]

K	Drag coefficient
L_c	Capillary length [m]
m	Wicking mass gain [g]
m_0	Wetting mass [g]
Oh	Ohnesorge number: Oh= $\sqrt{\rho\nu^2/\sigma D_h}$
P	Mesh perimeter [m]
P_p	Pore perimeter [m]
p	Pressure [Pa]
r^2	Correlation coefficient
R_e	Effective radius [m], $R_e = R_h^2/R_s$
R_h	Hydraulic radius [m], $R_h = A_p/P_p$
t	Experimental time [s]
t_c	Characteristic time [s]
T_m	Porous media thickness [m]
V	Volume fraction [-]
v	Flow velocity [m/s]
v_c	Characteristic velocity [m/s]: $v_c = \sqrt{4\sigma/\rho D_h}$
V_P	Pore volume [m^3]
V_m	Porous media volume [m^3]
W_m	Porous media width [m]
θ_s	Static contact angle [°]
Λ	Aspect ratio [-] $\Lambda = D_s/D_h$
μ	Dynamic viscosity [Pa s]
ν	Kinematic viscosity [m^2/s]: μ/ρ
ρ	Density [kg/m^3]
σ	Surface tension [N/m]
ϕ	Mesh porosity [-], $\phi = \mathrm{V}_P/\mathrm{V}_m$
Φ_w	Wicking pressure screen characteristic

State of the art

When a liquid ($\theta_s < 90°$) encounters a solid medium a rapid adhesion of the liquid to the external surface occurs. This process is called wetting. The wetting force is known from the Wilhelmy relation to be proportional to the contact angle, θ_s, formed between the solid and the liquid, the surface tension, σ, and the perimeter, $P = 2(W_m + T_m)$, of the mesh:

$$F_0 = P\sigma\cos\theta_s. \tag{1}$$

This leads to the mass involved in wetting:

$$m_0 = \frac{F_0}{g} = \frac{P\sigma\cos\theta_s}{g}. \tag{2}$$

The height of the static meniscus on the porous medium is given by [8]:

$$h_0 = L_c[2(1-\sin\theta_s)]^{1/2}. \tag{3}$$

where L_c is the capillary length:

$$L_c = \sqrt{\frac{\sigma}{\rho g}}. \tag{4}$$

Simultaneously, however slower than the wetting, a complex flow field develops within the pores of the mesh which is caused by wicking. The prediction of the wicking behavior depends on both the geometrical/physical properties of the mesh but also on the physical properties of the liquid. Many papers studied the spontaneous penetration of liquids into porous media and only few of them are summarized below.

Van Oss et al. [18], for example, determined the contact angles and pore sizes of porous media by column and thin layer wicking. They demonstrated that low-energy spreading liquids pre-wet the surface over which they subsequently spread. Siebold et al. [15] focused on total wetting liquids for which contact angles are zero at equilibrium. They showed that due to the rising velocity the contact angle is larger than expected, and proposed a new method to calculate the constant effective radius, R_e, in the Lucas-Washburn equation Eq.(8). A review article written by Bachmann et al. [3] describes the available methodologies for determining wetting properties of porous media. Chibowski et al. [4] also review existing literature on formulation and determination of surface free energy, and depict problems dealing with contact angles even with spreading liquids.

Theoretical studies of the rate of imbibition of porous media have also received significant attention. Many models of the pore space of porous media are based on some form of capillary tubes, this includes for example Washburn [19], who studied dynamic invasion of fluid into a capillary, Levine et al. [9], who examined the departure from Poiseuille flow in the vicinity of an advancing meniscus in a vertical cylindrical capillary, and Marmur [12], who showed the thermodynamic and kinetic effects on capillary penetration in systems of limited size. Symons [17] conducted a study to determine the magnitude of the wicking rates of liquids in various screens, including the one used in this study: Dutch-Twilled-Weave (DTW) 200×1400. An analytical model of the wicking process was developed, which expresses the wicking velocity as a function of liquid properties and geometric effects. Experimental data demonstrated that the model predicts the correct functional dependence of several parameters important in the wicking process. However, due to the complexity of the pore geometry within the screen, it was necessary to merge several screen geometric parameters into a single geometric constant.

Based on the momentum equation, Stange [16] claimed that the capillary rise process could be divided into four successive stages with an initial $h \sim t^2$ domain corresponding to the local acceleration of the liquid; a $h \sim t$ domain related to the convective acceleration, then a $h \sim \sqrt{t}$ behavior regarding the viscous molecular momentum transport, and finally a $h \sim 1 - e^{(1+t/h^2_{max})}$ behavior due to the gravity acceleration; each domain being separated by characteristic

times.
The inertia dominated flow regime has been - for example - examined by Quere [13]. For a later stage in capillary flow other authors [7, 17, 19] consider only the capillary pressure to be counteracted by the viscous momentum transport and the hydrostatic pressure. Wicking is therefore regarded as a process where the viscous forces dominate and the inertial forces can be neglected. For completeness cos θ_s is included in the following equations, however it approaches unity for perfectly wetting liquids. The momentum balance gives

$$\frac{4\sigma\cos\theta_s}{D_s} = \frac{32}{D_h^2}\mu h v + \rho g h. \tag{5}$$

The term on the left-hand side represents the capillary pressure across the liquid-vapor interface, which is a function of the surface tension and the static diameter. The first term of the right-hand side is the frictional pressure associated with viscous losses along the height of the wetted mesh while the last term represents the effect of gravity. In Eq.(5) the friction is expressed by the Hagen-Poiseuille model

$$\Delta p = \frac{32\mu h v}{D_h^2}, \tag{6}$$

which is valid for laminar flow. Also the porous medium is seen like a bundle of capillary tubes, while D_h includes the effect of arbitrary shaped pores. It shall be mentioned that the hydraulic diameter is defined as $D_h = 4R_h$. In this study the approach by Lucas [10] and Washburn [19] has been used. It allows to express the rate of liquid rise by

$$v = \frac{dh}{dt} = \frac{\sigma\cos\theta_s}{8\mu}\frac{D_h^2}{D_s}\frac{1}{h} - \frac{\rho g D_h^2}{32\mu}. \tag{7}$$

Neglecting gravity and solving Eq.(7) for the initial condition $h(t \to 0) = 0$ gives the well-known Lucas-Washburn equation:

$$h^2 = \frac{\sigma D_e \cos\theta_s}{4\mu}t = \frac{\sigma R_e \cos\theta_s}{2\mu}t, \tag{8}$$

with the effective diameter

$$D_e = \frac{D_h^2}{D_s}. \tag{9}$$

Eq.(8) can be modified to give the mass gain m instead of the height h:

$$m^2 = (T_m W_m \phi\ \rho)^2 \cdot \frac{\sigma D_e \cos\theta_s}{4\mu}t, \tag{10}$$

where ϕ is the porosity of the mesh. As mentioned before the Lucas-Washburn solution is only valid for flows with negligible inertia and gravity effects. According to Stange [16] at $t/t_c = 128(\mathrm{Oh}/\mathrm{Bo})^2$, with $t_c = D_h^2/(32\nu)$ being a characteristic time, gravity and friction are of same relevance. Thus Eq.(8) and Eq.(10) can only be applied for significantly smaller times. From the equations introduced previously it can be derived that for these times there will be a linear correlation between h^2 and t, respectively m^2 and t.
A full analytic solution of Eq.(5) is also given by Washburn [19] or Lukas and Soukupova [11], however in terms of $t(h)$ and not $h(t)$. One may define two constants:

$$a = \frac{\sigma\cos\theta_s}{8\mu}\frac{D_h^2}{D_s} \tag{11}$$

and

$$b = \frac{\rho g D_h^2}{32\mu}. \tag{12}$$

Solving the differential equation

$$\dot{h} = \frac{a}{h} - b \tag{13}$$

for the initial condition $h(t \to 0) = 0$ gives

$$t = -\frac{h}{b} - \frac{a}{b^2}\ln\left(1 - \frac{bh}{a}\right). \tag{14}$$

Dimensional analysis

To scale Eq.(7) it is appropriate to use the characteristic height $h_c = D_s$ and the characteristic velocity $v_c = \sqrt{4\sigma/(\rho D_h)}$. The velocity v_c was used by Stange [16] and others. With the dimensionless variables $h^* = h/h_c$ and $v^* = v/v_c$ Eq.(7) reads

$$\cos\theta_s = 16\Lambda^2 \mathrm{Oh} h^* v^* + \mathrm{Bo} h^*. \tag{15}$$

Three dimensionless groups appear in this equation: an aspect ratio $\Lambda = D_s/D_h$, the Ohnesorge number

$$\mathrm{Oh} = \sqrt{\frac{\rho\nu^2}{\sigma D_h}},$$

and the Bond number

$$\mathrm{Bo} = \frac{\rho g D_s^2}{4\sigma}.$$

Using this scaling, the experimental results merge into one master curve, as shown later (see Fig. 12).

EXPERIMENTAL

Experiments were performed with a mesh type (see Table 2) typical for the use within PMDs and test liquids with similar physical properties as typical propellants used in satellites.
To prevent any disturbing evaporation effects during the experiment only test fluids with a low vapor pressure have been used. The physical properties of the

Table 1: Fluid physical properties at 25 °C. The static contact angle, θ_s, between all test liquids and the mesh is near zero. The suppliers of the listed liquids are: 3M for HFE 7500 and FC-77, Dow Corning for Silicone Fluid 0.65.

		σ 10^{-3}	ρ	ν 10^{-6}	μ 10^{-3}
	Abbrev.	[N/m]	[kg/m^3]	[m^2/s]	[Pas]
SF 0.65	SF	15.4	758	0.64	0.49
HFE-7500	HFE	16.2	1610	0.77	1.24
FC-77	FC-77	16.3	1780	0.72	1.28

used liquids are summarized in Table 1. They all feature a near zero contact angle with the material used, giving $\cos\theta = 1$.
The porous screen is a Dutch-Twilled-Weave mesh (DTW) 200 × 1400 (Fig. 2); the numbers refer to the number of wires per inch in the warp/weft directions, see Table 2 for more details of the mesh. The mesh sample was laser-cut in rectangular shapes with precise dimensions ($H_m = 50$ mm by $W_m = 16$ mm) with the samples having the warp wires running perpendicular to the mesh width. Using the mesh rotated 90° (warp wires parallel to width) would also be possible, however the warp wires would induce a higher friction loss thus leading to a smaller hydraulic diameter. Evaluating the wicking in this mesh direction is a field of interest for further research.

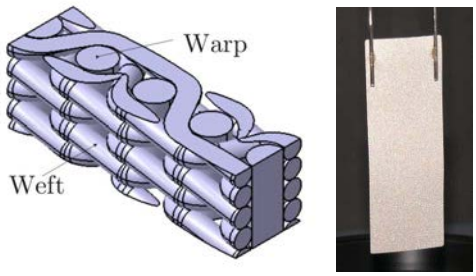

Figure 2: Drawing of the microstructure (left) and photography (right) of the Dutch-Twilled-Weave mesh (DTW) 200 × 1400 (supplier: Spoerl).

The microstructure quality of the meshes was checked using a microscope with a magnification that enables the detection of defects at the edges of the samples. Subsequently, the selected mesh underwent a cleaning protocol that removed any dust or grease left on the surface or in the interstices; this was performed using an ultrasonic bath with a metal cleaner Turco (supplier: Henkel).
Methods for measuring or predicting the porosity of a mesh are given by Armour and Cannon [2]. However for this work the "wicking effective porosity" was measured using following approach: the mesh was attached to a balance where the mass has been recorded for different wicking heights. Using the equation

$$m = T_m W_m \phi\ \rho h \tag{16}$$

the porosity could be calculated out of the slope (see Fig. 3) to be $\phi = 0.24 \pm 0.03$.

Table 2: Description of the Dutch-Twilled-Weave (DTW) 200 × 1400.

mesh metal	AISI 304 L (stainless steel)
200 × 1400	200 warp wires/inch 1400 weft wires/inch
warp wire diameter [μm]	70
weft wire diameter [μm]	40
H_m: test-mesh height [mm]	50±0.01
T_m: mesh thickness [μm]	149±1
W_m: test-mesh width [mm]	16±0.01

Table 3: Mesh properties defined experimentally

θ: porosity	0.24±0.03
D_e[μm], warp direction	3.38±0.2
D_s[μm], warp direction	27.4±1.9
D_h[μm], warp direction	9.62±0.4

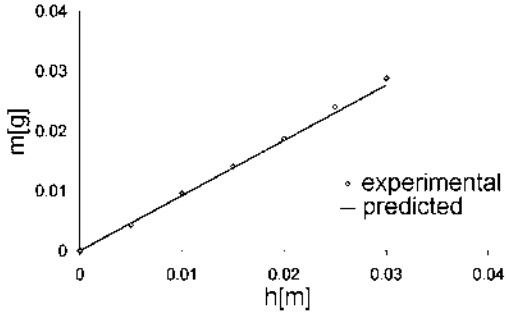

Figure 3: Graph of the liquid mass inside the wick plotted versus wicking height (HFE in 16 mm wide mesh)

Experimental setup

Fig. 4 displays an overview of the wicking experimental setup. In order to derive the wicking height video recordings were taken and analyzed with image processing software.
The setup consists of:

- a rectangular test chamber (50 mm wide), where the mesh was left hanging for 1 hour above the the liquid surface prior to the experiment start.

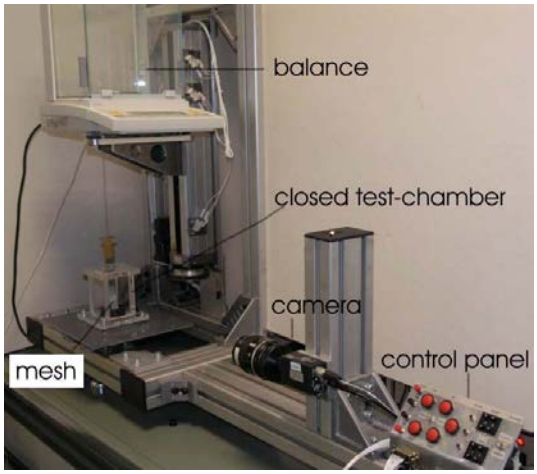

Figure 4: Photography of the wicking experimental setup.

During this period no increase in the mesh mass was recorded for all test liquids (accuracy of the balance ± 0.1 mg), which means no evaporation or capillary condensation occurred in the mesh. Fig. 5 describes the test assembly in more detail: the top of the test chamber is sealed with the bottom part, however there are two holes in the cover to allow the mesh being attached to the balance. Vapor diffusion through these holes may occur in varying strength. The mesh environment is therefore composed of air and vapor (concentration near saturation) of the test liquid.

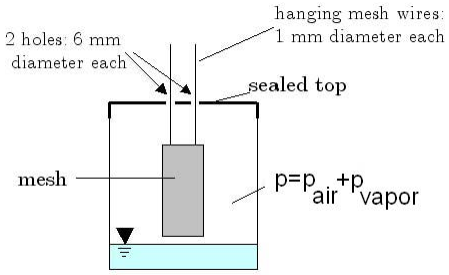

Figure 5: Sketch of the test chamber prior to wicking experiments.

- a camera used to record the liquid rise versus time within the mesh. The visualization of the wicking front was done with an analog camera set at 25 Hz, whereas the images have then been converted into digital ones in order to be analyzed by image processing software using Matlab features. At the liquid front line, a mean height out of each pixel along the total width of the mesh was then calculated with a standard deviation of ±5 pixel as shown in Fig. 6. The resolution of the camera and the lens gives 0.07418 mm/pixel.

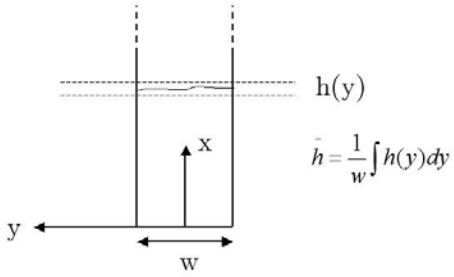

Figure 6: Mean height evaluation.

- an electronic balance with an accuracy of ±0.1 mg to which the mesh was attached by threads. The balance can be precisely and continuously moved up and down by means of an automated lift in order to get the mesh in contact with the test liquid at a constant velocity of 1 mm/sec. Data acquisition was controlled using Labview features.

A detailed sketch of the coordinate system is represented in Fig. 7 where the mesh is immersed in the test liquid.

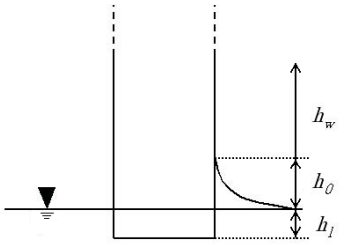

Figure 7: Definition of the height coordinates regarding the wicked mesh sample.

The height of the liquid front is the sum of three heights:

$$h = h_w + h_l + h_0, \tag{17}$$

where h_w is the height due only to the wicking process; h_l is the immersion depth of the mesh in the liquid, this is a safety length to ensure that the total width of the mesh is in contact with the test liquid (in case if the bottom part of the mesh was not completely parallel to the test liquid surface): $h_l = 0.55$ mm. h_0 is the height of the mesh covered by the liquid due to the wetting phenomenon and is given by Eq. (3).

To point out the chronological development of an experiment a curve of mass measurement versus time is shown in Fig. 8. The curve is divided in six parts, describing the mesh from the imbibition to the drying.

At first, the mesh is brought into contact with the test

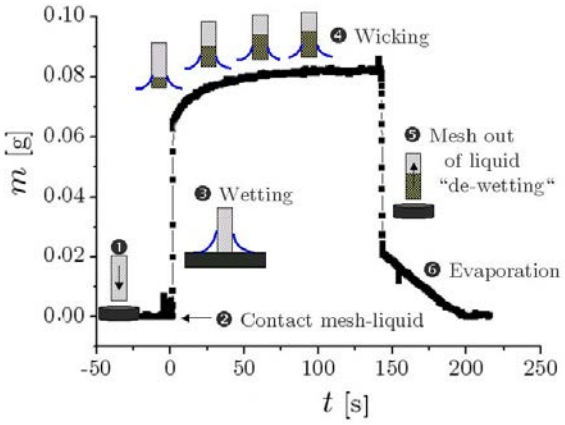

Figure 8: Description of the mass versus time curve (open test chamber). Imbibition of a mesh (50x16) by HFE.

liquid inducing the wetting process, as expressed by Eq.(2).
The liquid will then start to wick into the mesh, while the mass will increase to finally reach a plateau value. In ideal conditions (i.e. no evaporation), this responds to the equilibrium state between the capillary and the hydrostatic pressures. Finally, the last step displays the liquid evaporation trend out of the mesh which will only take place in unsaturated environments (open test chamber). It is worth noting that the evaporation is a fairly linear process.

Evaluation of experimental results

To extract mesh parameters out of experimental results the linear behavior of h^2 respectively m^2 over t can be used. Taken from Eq.(8) and (10), the effective diameter D_e can be extracted out of the curve's slope. However, this is only possible as long as the influence of gravity is small. The focus of this work is the evaluation of height measurements. A subsequent series of images showing wicking is presented in Fig. 9, where similar series have been used to gain the height values.

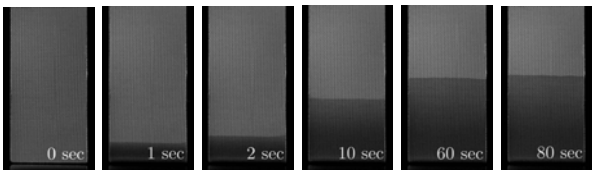

Figure 9: Wicking of the mesh using HFE for increasing time.

Fig. 10 shows the experimental results, where the height is plottet versus time using three test liquids and a 16 mm wide screen. It is observed that there

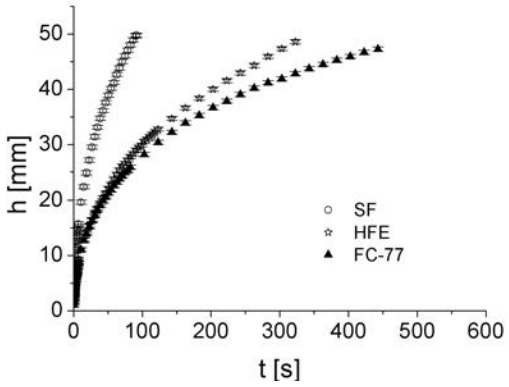

Figure 10: Wicking height raw data with error bars (standard deviation is ±5 pixel).

is a strong rise in the beginning of the measurement which decreases with the time.

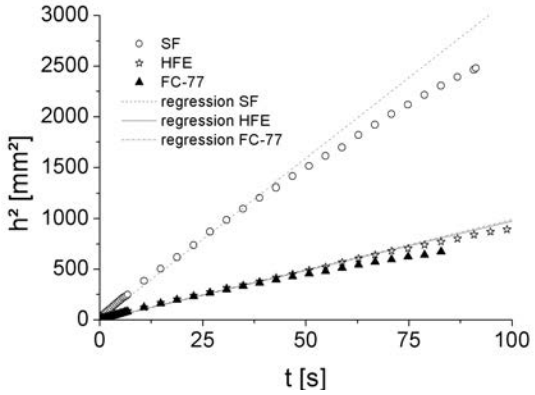

Figure 11: Height^2 over time with linear fitting (no error bars for graph clarity).

In Fig. 11, the squared height is plotted versus time. Near the origin a linear slope can be seen, where the regression has been done using the method of least squares. Table 4 contains the D_e results for different fluids and their correlation coefficient.
From Table 4 it can be seen that there is a small deviation between the measurements made with the different liquids. The average is $D_e = 3.38$ μm with an correlation coefficient of 0.995. Comparing this result with literature, for example Dodge [5] who obtains $D_e = 2.72$ μm verifies the results to some extent. He cites [6] as a source, where evaporation is not suppressed during the experiment. Thus, the higher evaporation rate may explain the smaller effective diameter. Dodge does not use the static, effective and hydraulic diameters but other material factors and friction coefficients, though they can be converted to the

Table 4: D_e calculated from height measurements. Number in brackets are correlation coefficients r^2. D_h calculated with $D_s = 27.4$ μm.

	D_e (experimental) [μm]	D_h (calculated from D_e) [μm]
SF	4.00 (0.995)	10.48 ±0.4
HFE	2.98 (0.997)	9.04 ±0.4
FC-77	3.16 (0.992)	9.31 ±0.4
Average	3.38 (0.995)	9.62 ±0.4

diameters by following correlations

$$\frac{\Phi_w}{D_{\mathrm{BP}}} = \frac{4}{D_s} \tag{18}$$

and

$$\frac{C_w}{B_s^2} = \frac{32}{D_h^2}. \tag{19}$$

Dodge also mentions a scatter of experimental results of different publications.
If one likes to further investigate the effective diameter D_e, which can be rendered more precisely by two other diameters, namely the static diameter D_s and the hydraulic diameter D_h (see Eq.(9)), one has to conduct a second experimental analysis.
By evaluating the maximum height, $h_{\max}$, achievable when the liquids stop rising due to the equilibrium between the capillary and the gravity forces, the static diameter D_s can be calculated and thus, knowing D_e, the hydraulic diameter D_h. In order to measure $h_{\max}$ an additional larger scale setup has to be used, as $h_{\max}$ (depending on the liquid) was larger than the initial test setup size. The larger setup did not feature a balance, but was sealed to prevent any evaporation. The results gave $D_s = 27.4 \pm 1.9$ μm. Dodge [5] states $D_s = 176$ μm which is a fairly high discrepancy. The sensitivity of the experiment to evaporation may explain this difference. Dodge's [5] values can be converted to $D_h = 21.88$ μm, which also deviates through the strong difference in his D_s.

Table 5: Maximum height estimated when capillary and hydrostatic pressure balance and no evaporation occurs.

	$h_{\max}$ [mm]
SF	296
HFE	150
FC-77	136

It shall be mentioned that measurements are also conducted using meshes with different widths ranging from 10 to 18 mm. Comparing the results shows no significant influence of the width.

The experimental data in Fig. 10 is scaled with the characteristic numbers derived in the theoretical section, namely the Oh number and the Bo number. Fig. 12 shows the characteristic height scale versus the characteristic time scale for the experimental points and a numerical solution of Eq.(15). The data collapses to one master curve. This confirms the relevance of the non dimensional numbers to characterize the wicking behavior, but also enables the prediction of any other liquid front line height. The validity of numerical results applies approximately from t/t_cOh equal 3×10^4 to 1×10^7, while the lack of coincidence below 3×10^4 could be explained by the difficulty to get precise height values at the beginning of the wicking phenomenon due the overlapping between wetting and wicking.

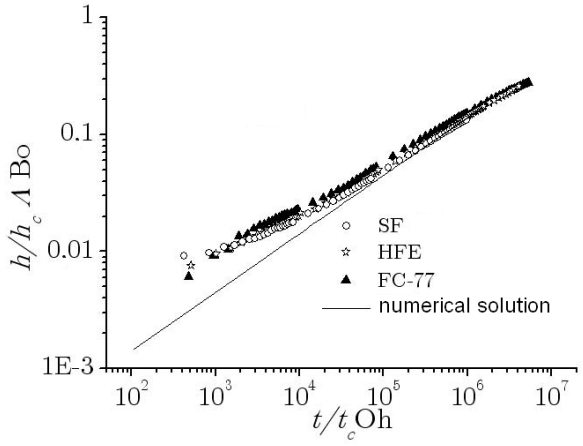

Figure 12: Dimensionless representation of the experimental and numerical (Eq.(15)) results for the test liquids.

NUMERICAL SIMULATION

To analyze the wicking of liquids into more challenging geometries of screens either experiments have to be conducted for each application, or a numerical simulation can be performed. Prior to having a reliable simulation tool a simple test case has to be simulated. Comparing the numerical results with experimental results allows to verify the model including the parameters. For this case the commercial CFD software FLOW-3D is used. This application is able to run a direct microscopic simulation of the wicking process as it occurs in porous media. For this kind of setup it is necessary to import the exact geometry of the mesh with the individual pores and to define the surface tension, surface contact angle, density and viscosity of the liquid. Using free surface calculation methods the solver can simulate the wicking in every single pore. This technique, however, has some limitations, in particular when it comes to the simulation of a complete screen

and not just an elementary cell. Due to the limited size of the pores (some μm) in comparison to the overall screen size (50 mm) large numbers of meshing cells are necessary to make up the individual pores and their characteristic geometry. Even when using new computer hardware the available calculation power is not sufficient to simulate wicking within reasonable time (allowance max. several days calculation time).

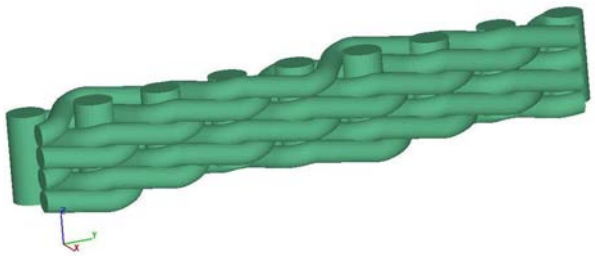

Figure 13: Digital representation of the screen showing its microscopic structure.

To solve this problem FLOW-3D features a macroscopic porosity model. This model does not simulate the wicking of the liquid into the individual pores, since it uses capillary pressure and flow resistance models to calculate the overall behavior of a porous medium in contact with a wetting liquid. FLOW-3D solver 9.0.2 and interface 9.0.3 are used, utilizing the incompressible, one fluid model with gravity effects (when desired). As the frontier between wetted and dry screen is sharp, no unsaturated flow occurs. So, choosing the volume fraction dependent model is a possible option for wicking simulation. This model uses the following drag correlation: The momentum loss due to friction within the porous medium is $-Kv$. Here v is the flow velocity and K is a drag coefficient. For the volume fraction dependent model:

$$K = aV^{-b}, \tag{20}$$

where a and b are constants. Setting b to 0 renders K independent of the volume fraction V and thus gives a constant factor $K = a$. When using the Poiseuille drag model

$$\Delta p = \frac{32\mu h v}{D_h^2} \tag{21}$$

and taking into account the momentum equation used in FLOW-3D gives:

$$a = \frac{32\mu}{\rho D_h^2}. \tag{22}$$

Considering these coefficients, the porosity and the capillary pressure can be entered in the porous media folder under "meshing and geometry". The initial condition is a dry mesh, where the boundary condition includes one boundary with fluid fraction set to one, thus simulating the contact with a liquid reservoir.

After the simulation is finished the results can be analyzed and compared to the predicted values. First of all, it is worth noting that the fluid volume which enters the screen is the main output parameter as it can be related to the wicking height and the fluid mass. Fig. 14 shows a mass vs. time plot of the FLOW-3D simulations (with and without gravity) in comparison to the predicted values of the Lucas-Washburn equation and a numerical solution of the differential equation Eq.(5) including the gravity term. A very good consistency can be seen, where the numerical data deviates minimally to lower values. This may be traced back to the inertia term which is taken into account in the FLOW-3D setup, while the Lucas-Washburn equation and Eq.(5) do not include it.

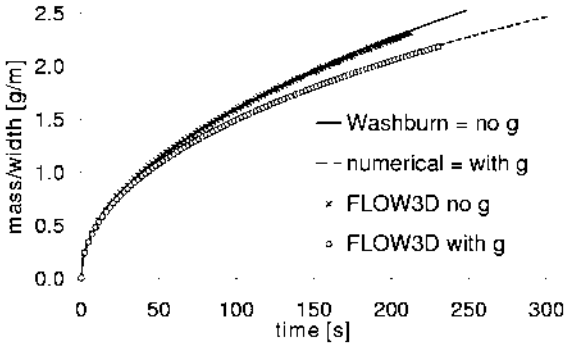

Figure 14: Diagram of fluid volume inside the screen versus time.

CONCLUSIONS

The wicking behavior of perfectly wetting liquids in metallic meshes are studied. By means of the momentum balance the Lucas-Washburn equation and further analytical solutions are introduced. The dimensionless Ohnesorge and Bond numbers are then found to be relevant to characterize the liquid progress into the mesh. An experimental setup using a vertical positioned mesh is used to investigate the wicking behavior of different liquids. The experimental results, namely the height recordings, are compared with analytical solutions. Good agreement between the Lucas-Washburn equation and the experimental data is found for flow regimes where gravity effects are negligible. From these characteristic pore parameters could be determined. The results for the effective diameter are validated by previous literature, however, there are discrepancies for the static diameter which may occur due to the sensitivity of the experiment to evaporation. Using the introduced dimensionless numbers all experimental data collapses to a single curve supporting the theoretical model. Furthermore a method for numerical simulations of liquid wicking into a porous medium

is introduced. Finally, the experimental setup can be expanded for investigations of further porous media, evaporation effects and cryogenic liquids.

ACKNOWLEDGEMENT

The funding of the research project by the German Federal Ministry of Education and Research (BMBF) through the German Aerospace Center (DLR) under grant number 50JR0011 and the Deutsche Forschungsgemeinschaft through the Research Training Group PoreNet is gratefully acknowledged. The authors also like to gratefully acknowledge the support of Spoerl.

References

[1] B.N. Antar and V.S. Nuotio-Antar. *Fundamentals of Low Gravity Fluid Dynamics and Heat Transfer*, chapter Chapter 9, pages 265–287. CRC Press, Boca Raton, Florida, 1993.

[2] J.C. Armour and J.N. Cannon. Fluid flow through woven screens. *AICHE Journal*, 14(3):415–420, 1968.

[3] J. Bachmann, S. K. Woche, M.O. Goebel, M.B. Kirkham, and R. Horton. Extended methodology for determining wetting properties of porous media. *Water Resour. Res.*, 39(12), 2003.

[4] E. Chibowski and R. Perea-Carpio. Problems of contact angle and solid surface free energy determination. *Advances in colloid and interface science*, 98:245–264, 2002.

[5] F. T. Dodge. *The new Dynamic behavior of Liquids in Moving Containers*. Southwest Research Institute, San Antonio, Texas, 2000.

[6] F. T. Dodge and E. B. Bowles. Vapor flow into a capillary propellant-acquisition device. In AIAA, editor, *19th Joint Propulsion Conference*, number AIAA-83-1380, pages 1–9, Seattle, Washington, June 1983.

[7] F.T. Dodge. *Low-Gravity Fluid Dynamics and Transport Phenomena*, volume 130, chapter 1, pages 3–14. Aeronautics and Astronautics, Washington, DC, 1990.

[8] L. D. Landau and E. M. Lifschitz. *Lehrbuch der Theoretischen Physik, Band VI, Hydrodynamik*. Akademie Verlag, Berlin, 1991.

[9] S. Levine, J. Lowndes, E. J. Watson, and G. Neale. A theory of capillary rise of a liquid in a vertical cylindrical tube and in a parallel-plate channel. *J. Colloid Interf. Sci.*, 73(1):136–151, January 1980.

[10] Richard Lucas. Ueber das Zeitgesetz des kapillaren Aufstiegs von Flüssigkeiten. *Kolloid-Zeitschrift*, 23:15–22, 1918.

[11] D. Lukas and V. Soukupova. Recent studies of fibrous materials wetting dynamics. *In INDEX 99 Congress, Geneva, Switzerland*, 1999.

[12] A. Marmur. Penetration and displacement in capillary systems of limited size. *Adv. Colloid Interfac.*, 39:13–33, April 1992.

[13] D. Quere. Inertial capillarity. *Europhys. Lett.*, 39(5):533–538, July 1997.

[14] J.R. Rollins, R.K. Grove, and D.E. Jaekle. Twenty-three years of surface tension propellant management system design, development, manufacture, test, and operation. In AIAA, editor, *21st Joint Propulsion Conference*, pages 1–9. AIAA-85-1199, 1985.

[15] A. Siebold, M. Nardin, J. Schultz, A. Walliser, and M. Oppliger. Effect of dynamic contact angle on capillary rise phenomena. *Colloids and Surfaces A*, 161(1):81–87, January 2000.

[16] M. Stange. *Dynamik von Kapillarströmungen in Zylindrischen Rohren*. PhD thesis, Universität Bremen, Fachbereich Produktionstechnik, 2004.

[17] E.P. Symons. Wicking of liquids in screens. *NASA TN D-7657*, 1974.

[18] C. van Oss, R. Giese, Z. Li, K. Murphy, J. Norris, M. Chaudhury, and R. Good. Determination of contact angles and pores sizes of porous media by column and thin layer wicking. *J. Adhesion Sci. Technol.*, 6(4):413–428, 1992.

[19] E.W. Washburn. The dynamics of capillary flow. *Physical Review*, 17(3):273–283, 1921.